CELL BIOLOGY

Mechano-gradients drive morphogen-noise correction to ensure robust patterning

Kana Aoki[1], Taiki Higuchi[1], Yuki Akieda[1], Kotone Matsubara[1], Yasuyuki Ohkawa[2], Tohru Ishitani[1,3]*

Morphogen gradients instruct cells to pattern tissues. Although the mechanisms by which morphogens transduce chemical signals have been extensively studied, the roles and regulation of the physical communication between morphogen-receiver cells remain unclear. Here, we show that the Wnt/β-catenin–morphogen gradient, which patterns the embryonic anterior-posterior (AP) axis, generates intercellular tension gradients along the AP axis by controlling membrane cadherin levels in zebrafish embryos. This "mechano-gradient" is used for the cell competition–driven correction of noisy morphogen gradients. Naturally and artificially generated unfit cells, producing noisy Wnt/β-catenin gradients, induce local deformation of the mechano-gradients that activate mechanosensitive calcium channels in the neighboring fit cells, which then secrete annexin A1a to kill unfit cells. Thus, chemo-mechanical interconversion–mediated competitive communication between the morphogen-receiver cells ensures precise tissue patterning.

INTRODUCTION

During tissue patterning, the fate of each cell is governed by chemical signaling networks activated by secreted morphogens (*1*–*3*). In addition to chemical signaling, "mechanical force" also plays an essential role in tissue pattern formation (*4*–*6*). Mechanical force, defined as the cellular contractile force generated by actomyosin (*7*) and the viscoelasticity of cells (*8*), drives tissue morphogenesis. For instance, actomyosin-driven contractions drive crypt morphogenesis (*9*). Local intercellular tension heterogeneity drives organ-scale patterning and cell fate decisions during cardiac trabeculation (*10*). The feedback mechanisms controlling the interactions between chemical signaling and mechanical force are gradually being understood because such interactions were first reported by D'Arcy Thompson a century ago (*11*). Morphogens are chemical substances that instruct cells to adopt suitable fates for tissue patterning by forming signaling activity gradients (*1*–*3*). The mechanisms by which morphogens transduce chemical signals have been extensively studied using animal genetic and biochemical analyses (*12*–*14*). However, the role of physical communication between morphogen-receiving cells during morphogen gradient formation has not been well studied. Here, we show that "chemical signaling gradients" formed by Wnt morphogens, which regulate brain anterior-posterior (AP) patterning, are converted to "mechano-gradients" generated via actomyosin contractile activity. Using mechano-gradients, unfit cells producing substantial noise in the Wnt morphogen gradient are sensed and eliminated by the neighboring fit cells. This chemo-mechanical and mechanochemical conversion drives the cell competition–mediated correction of noisy morphogen gradients that maintain robust tissue patterning.

RESULTS

Wnt/β-catenin gradients generate mechano-gradients

Previously, we showed that Wnt/β-catenin signaling posttranslationally stabilizes β-catenin and E-cadherin proteins in the plasma membrane, thereby generating membrane gradients of β-catenin and E-cadherin along the AP axis in the dorsal part of zebrafish embryos (Fig. 1, A and B) (*15*). The cadherin-catenin system is linked to cell-cell adhesion and the actomyosin system, which generates tensile force between adherent cells (Fig. 1C) (*16*–*18*). An increase in membrane E-cadherin levels can activate actomyosin and increase intercellular tensile forces (*19*). Therefore, we hypothesized that the β-catenin and E-cadherin membrane gradients affect intercellular tensile forces in zebrafish embryos. To test this hypothesis, we visualized actomyosin contractility using phalloidin (F-actin) and phosphorylated myosin-light-chain (p-MLC) immunostaining. F-actin and p-MLC membrane gradients were detected along the AP axis (Fig. 1B), suggesting that gradients of actomyosin contraction activity are formed in the same manner as those of Wnt/β-catenin and E-cadherin. Subsequently, we examined the distribution of activated RhoA as an indicator of actomyosin contractility because RhoA is a small G protein, which is activated to increase actomyosin contractility by activating Rho-kinase (ROCK) (*20*) at cell-cell junctions that generate a tensile force between cells (*21*). A RhoA biosensor, which helps in visualizing RhoA activity by specifically binding to RhoA–guanosine 5′-triphosphate (*22*), was strongly activated in the plasma membrane in the posterior area but not in the anterior area (Fig. 1D), suggesting that membrane RhoA-mediated intercellular gradients are formed along the AP axis. To confirm whether intercellular tension gradients are formed, we performed laser dissection (*23*) using a modified protocol of a conventional method that quantifies the speed of relaxation of dissected wounds. We quantified the width of a dissected wound after laser cutting. Zebrafish embryos consist of an epithelial envelope layer (EVL) and mesenchymal tissues (deep cells) (*24*). In both the EVL and deep cells, the width of the dissected wound in the posterior area was significantly longer than that in the anterior area (Fig. 1E), suggesting that intercellular tension gradients formed along the AP axis in both EVL and deep cell tissues. We named this gradient "mechano-gradient," which is defined as the gradient of actomyosin contractile force generated by the difference in cell-cell adhesion depending on Wnt signaling activity along the AP axis in the embryonic dorsal tissue.

Subsequently, we examined the relationship between Wnt/β-catenin, E-cadherin, and mechano-gradient. Forced activation of

[1]Department of Homeostatic Regulation, Research Institute for Microbial Diseases, Osaka University, 3-1 Yamadaoka, Suita, Osaka 565-0871, Japan. [2]Division of Transcriptomics, Medical Institute of Bioregulation, Kyushu University, 3-1-1 Maidashi, Fukuoka, Fukuoka 812-0054, Japan. [3]Center for Infectious Disease Education and Research (CiDER), Osaka University, 3-1 Yamadaoka, Suita, Osaka 565-0871, Japan.
*Corresponding author. Email: ishitani@biken.osaka-u.ac.jp

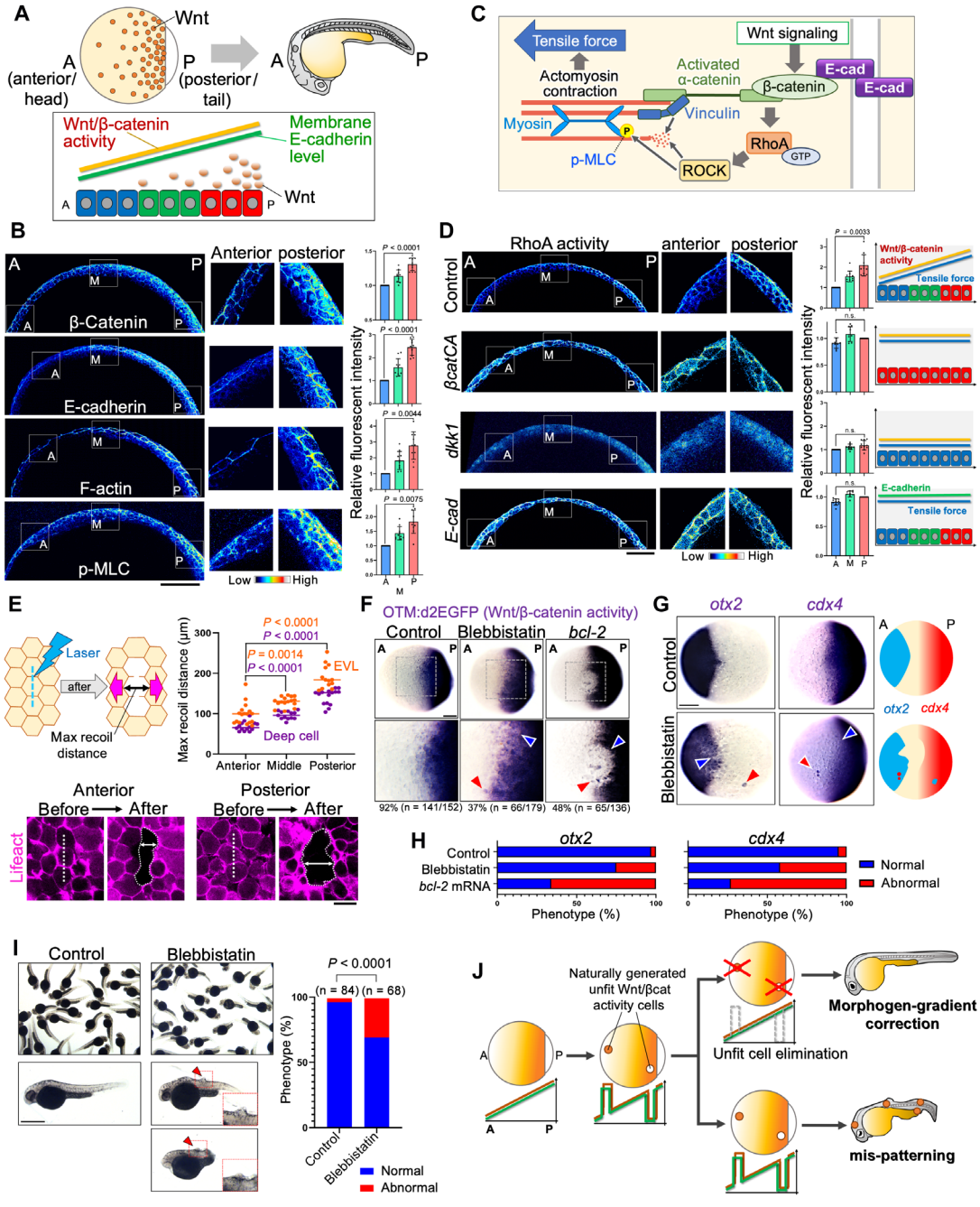

Fig. 1. Wnt/β-catenin gradient generates mechano-gradient. (**A**) Wnt/β-catenin activity gradient formation. (**B**) Membrane β-catenin, E-cadherin, F-actin, and p-MLC protein levels. Optical sagittal cross sections (dorsal side) of 8-hpf embryos. Scale bar, 50 μm. Right: Means ± SD; $n = 10$ embryos; across anterior-posterior (AP) axis. Relative fluorescent intensity in the anterior (A), central middle (M), and posterior (P) regions shown in the images on the left was quantified. (**C**) Wnt signaling and cortical actomyosin contraction underneath adherence junction. (**D**) RhoA activity gradients. Tg (HS:GFP-βcatCA) or Tg (HS:dkk1b-GFP) and E-cadherin–mRNA–injected zebrafish embryos and sibling embryos at 9 hpf. Scale bar, 50 μm. Right: Means ± SD; $n = 10$ embryos. Relative fluorescent intensity in the anterior (A), central middle (M), and posterior (P) regions was quantified. n.s., not significant. (**E**) Left: Laser dissection method. Bottom: Embryos injected with Ruby-Lifeact mRNA (magenta) before and after laser dissection. White arrows: Maximum recoil distances in (right) anterior, central middle, and posterior tissues. Scale bar, 20 μm. EVL, epithelial envelope layer (orange); deep cells (purple). Means ± SD ($n = 31$, 29, and 28 experiments). (**F**) d2EGFP in Wnt/β-catenin reporter (OTM:d2EGFP)–transgenic embryos (dorsal view) treated with DMSO (control) or 2.5 μM blebbistatin or injected with *bcl-2* mRNA. Red arrowheads: Abnormally high or low Wnt/β-catenin activity. Scale bar, 200 μm. (**G**) *otx2* and *cdx4* markers in embryos treated with DMSO (control) or 2.5 μM blebbistatin. Scale bar, 200 μm. Left: AP tissue marker expression. (**H**) Percentage of embryos with normal or abnormal expression patterns ($n = 100$). Two-tailed one-way analysis of variance (ANOVA). (**I**) Zebrafish larvae (32 hpf) treated with DMSO (control) or 2.5 μM blebbistatin from 6 to 9 hpf. Red arrowheads: Abnormal cell proliferation. Scale bar, 500 μm. Right: Percentages of embryos with normal or abnormal morphology. The total number of embryos analyzed are shown above the graph (Fisher's exact test). (**J**) Naturally generated "noise" cells are eliminated via E-cadherin gradient formation.

Wnt/β-catenin signaling by constitutively active β-catenin (βcatCA) and overexpression of E-cadherin in whole embryos increased membrane RhoA activity in the anterior region, where endogenous Wnt/β-catenin activity and membrane E-cadherin levels are low (Fig. 1D). However, overexpression of the Wnt antagonist Dkk1, which inhibits Wnt/β-catenin activity, reduced membrane RhoA activity (Fig. 1D). Laser dissection experiments revealed that activation and inhibition of Wnt/β-catenin activity increased and decreased intercellular tensile force in the embryos, respectively (fig. S1A), suggesting that the mechano-gradient is formed downstream of Wnt/β-catenin signaling. Together, Wnt/β-catenin activity generates actomyosin contractile force by regulating membrane E-cadherin levels, and, thus, a mechano-gradient along the AP axis is formed in a Wnt/β-catenin activity–dependent manner.

Mechano-gradient contributes to unfit cell elimination

To determine the physiological role of the mechano-gradient generated by Wnt/β-catenin–mediated actomyosin contraction, embryos were treated with the myosin inhibitor blebbistatin to inhibit mechano-gradient formation. Embryos treated with 2.5 μM blebbistatin showed no gross morphologic abnormalities during early embryogenesis (fig. S1B). However, this treatment blocked mechano-gradient formation (fig. S1C) and induced ectopic activation and abnormal reduction of the Wnt/β-catenin reporter (Fig. 1F and fig. S2, A and B). Moreover, ectopic expression of the anterior brain marker *otx2* was detected in the posterior region, and the posterior brain marker *cdx4* was ectopically activated in the anterior region (Fig. 1, G and H, and fig. S2, A, and B). Disruption of the mechano-gradient by blebbistatin treatment also disturbed embryonic morphogenesis (Fig. 1I). These results suggest that the mechano-gradient is necessary for proper formation of the Wnt/β-catenin morphogen gradient and brain AP pattern and precise embryogenesis.

We previously reported that unfit cells with abnormally high or low Wnt/β-catenin activity producing the noises in the Wnt/β-catenin morphogen gradient along the AP axis are naturally generated in zebrafish embryogenesis. However, these unfit cells are eliminated through cell competition with neighboring normal cells (*15*). The conversion of Wnt/β-catenin activity into E-cadherin levels plays an essential role during this elimination of unfit cells. The abnormally high or low Wnt/β-catenin activity in the unfit cells is, respectively, converted to abnormally high or low membrane E-cadherin levels, which generates an imbalance in E-cadherin levels between unfit cells and neighbors, thereby inducing the activation and nuclear translocation of transforming growth factor–β (TGF-β)–type Smad (Smad2/3/4) and degradation of anti-apoptotic Bcl-2 proteins, consequently resulting in apoptosis of the unfit cells (*15*). Inhibition of this cell competition by overexpressing *bcl-2* causes unfit cell accumulation and consequent disruption of proper AP patterning and embryonic morphogenesis (Fig. 1, F and H) (*15*). Similar to this inhibition of unfit cell elimination, blebbistatin treatment disrupts AP pattern formation, suggesting that the mechano-gradient may also be involved in the elimination of the unfit cells and the noise correction of the Wnt/β-catenin gradient (Fig. 1J). To test this possibility, we artificially introduced a small number of fluorescent protein (mKO2)–Wnt/β-catenin–expressing abnormal cells into zebrafish embryos by injecting heat-shock–driven expression plasmids (Fig. 2A) and examined their elimination. As previously reported (*15*), the artificially introduced unfit cells with abnormally high or low Wnt/β-catenin activity, which overexpress βcatCA or Axin1 (a Wnt/β-catenin–negative regulator), respectively, activated caspase-3 (Fig. 2B), an indicator of apoptosis. The inhibition of TGF-β–type Smad activation in the whole embryo blocked the apoptotic elimination of unfit cells with Wnt/β-catenin activity (fig. S3A), indicating that Smad is a critical mediator of unfit cell apoptosis, as we previously reported (*15*). Inhibition of mechano-gradient formation by blebbistatin treatment blocked caspase-3 activation in these unfit cells (Fig. 2B). Blebbistatin treatment also prevented the activation of Smad2 in the Wnt/β-catenin–unfit cells (fig. S3B). Similar to that observed after blebbistatin treatment, treatment with Y27632, which is a chemical inhibitor of the actomyosin activator ROCK, blocked mechano-gradient formation (fig. S1C) and activation of Smad2 and caspase-3 in the Wnt/β-catenin–unfit cells (fig. S3, B and C). In addition, the up-regulation of actomyosin contractile force via RhoA-ROCK activation in whole embryos by treatment with the chemical activator of RhoA (CN03) also suppressed unfit cell apoptosis (fig. S3D). These results suggest that the mechano-gradient is required for Smad activation and subsequent apoptosis in the Wnt/β-catenin–unfit cells.

Local tension change drives unfit cell elimination

How does the mechano-gradient contribute to the apoptosis of unfit cells? We previously showed that unfit cells with abnormally high or low Wnt/β-catenin activity induce up-regulation or down-regulation of membrane E-cadherin levels, respectively, which stimulates Smad activation and consequent apoptosis in unfit cells (*15*). However, the mechanisms through which changes in E-cadherin levels activate Smad in unfit cells remain unclear. Because Wnt/β-catenin activity is converted to tensile force via regulation of E-cadherin levels in zebrafish embryos, we hypothesized that tensile force acts downstream of E-cadherin in unfit cell elimination. As expected, mosaically introduced Wnt/β-catenin–hyperactivated cells increased RhoA activity and E-cadherin, F-actin, and p-MLC levels in the membrane in the anterior area, whereas Wnt/β-catenin–inhibited cells significantly reduced these levels in the posterior area (Fig. 2C and fig. S3, E to G). Blebbistatin treatment blocked these p-MLC ectopic increases and decreases (fig. S3G). Cells overexpressing E-cadherin showed increased F-actin levels and RhoA activity in the anterior area with low F-actin and RhoA levels (fig. S3, F and H). Conversely, E-cadherin knockdown blocked this RhoA activation in Wnt-hyperactivated cells (fig. S3I). These results suggest that unfit cells with abnormally high or low Wnt/β-catenin activity increase or decrease RhoA-actomyosin activity, respectively, through E-cadherin. Overall, the Wnt/β-catenin signaling activity of unfit cells is likely to cause local tension changes.

To further investigate the involvement of local tension changes in unfit cell elimination, we modified the activities of tension regulators, including α-catenin, RhoA, and ROCK. The tensile force applied to adherence junctions converts α-catenin from a closed structure to an "open structure" to expose its vinculin binding site, and, thereby, vinculin is recruited to adherens junctions to enhance cortical actomyosin localization and consequent activation (Fig. 1C) (*25*). Overexpression of conformationally active α-catenin mutant (M319G/R326E; αcatCA) (fig. S4A), which constitutively activate actomyosin underneath adherens junction via vinculin recruitment (*25*–*28*), increased tensile force in embryos (fig. S4, B and C). Mosaic introduction of αcatCA–expressing cells activated nuclear translocation of Smad2 (fig. S4D) and caspase-3 efficiently in the anterior region where Wnt/β-catenin signaling activity and actomyosin contractile forces are low but not in the posterior region where these activities are relatively high (fig. S4, E and F). In contrast, the ubiquitous introduction of αcatCA–expressing cells did not activate apoptosis (fig. S4E). In addition, cells overexpressing wild-type α-catenin did not activate caspase-3 (fig. S4G). These results suggest

that cells with abnormal α-catenin activity undergo apoptosis in a manner dependent on neighboring normal cells. To further examine the importance of force-detection ability by α-catenin, we introduced L344P point mutation, which blocks the binding of α-catenin to vinculin (*29*, *30*), to αcatCA (fig. S4A). Mosaically introduced αcatCA+L344P-overexpressing cells survived (fig. S4G), suggesting that mechanical force–dependent conformational change of α-catenin is required for initiating cell competition–mediated unfit cell elimination. Similar to that in abnormal Wnt/β-catenin hyperactivated cells, RhoA activity was increased in αcatCA cells (fig. S3H). Treatment with a ROCK inhibitor, Y27632, which decreased tensile force in embryos (fig. S1C), blocked αcatCA cell apoptosis (fig. S4H). Overexpression of αcatCA inhibited apoptotic elimination of Wnt/β-catenin–inhibited cells (fig. S4I), suggesting that local tension change was required for triggering cell competition.

Next, we induced unfit cells expressing a constitutively active RhoA mutant (Q63L; RhoACA) or dominant-negative RhoA mutant (T19N; RhoADN), which increased or decreased tensile force, respectively, in embryos (fig. S4, B and C), and confirmed that Smad2 and caspase-3 were activated in these cells with abnormal RhoA activity (Fig. 2D and fig. S4D). The inhibition of TGF-β–type Smad activation in whole embryos blocked caspase-3 activation of RhoACA-expressing cells (fig. S4J). Similar to that in αcatCA-expressing cells, RhoACA-expressing cells efficiently underwent apoptosis in the anterior area where Wnt/β-catenin and actomyosin activities were low, but not in the posterior area where these activities were high (Fig. 2D). In contrast, RhoADN cells underwent efficient apoptosis in the posterior area but not in the anterior area (Fig. 2D). These results indicate that the local tension change was sufficient to trigger Smad activation and the consequent elimination of unfit cells. Moreover, the local tension change caused by abnormal Wnt/β-catenin activity triggered cell competition–mediated unfit cell elimination via RhoA-mediated actomyosin contraction.

Local tension change may apply mechanical stress to neighboring cells

To confirm that actomyosin contractile force change in unfit cells with abnormal Wnt/β-catenin activity causes mechanical stress to neighboring cells, we examined whether unfit cell–induced local tension changes affected the movement of neighboring normal cells. We examined the angle at which the centroid of neighboring cells moved relative to the centroid of unfit cells (fig. S5A). Neighboring control cells moved in random directions, and no bias in distribution was observed in the histogram (fig. S5B). However, in the presence of unfit cells with abnormally high or low Wnt/β-catenin activity, the movement of neighboring cells shifted to a direction parallel to that of the abnormal cells (fig. S5B), suggesting that Wnt/β-catenin–unfit cells may apply mechanical stress on neighboring cells and restrict their movement direction: Wnt-hyperactivated cells with increased-actomyosin contractile force pull neighboring cells toward themselves while neighboring cells are pulled in the opposite direction to Wnt-inhibited cells with decreased-contractile force compared to the surrounding tissue. Next, we quantified the change in distance between the centroids of the neighboring and unfit cells. Compared to that for control cells, the distances moved by neighboring cells increased in the presence of unfit cells with both abnormally high and low Wnt/β-catenin activities (fig. S5C). Furthermore, the appearance of Wnt-hyperactivated unfit cells significantly increased the movement of neighboring cells toward unfit cells (Fig. 2, E and F). In contrast, the neighboring cells moved away from Wnt-inhibited unfit cells (Fig. 2, E and G), suggesting that mechanical stress may be applied to neighboring cells in response to the appearance of Wnt/β-catenin–unfit cells (Fig. 2H).

Mechanical stress activates calcium channels in neighboring cells

How is mechanical stress converted into chemical signals that induce cell competition? One possible candidate is the mechanosensitive calcium channels, which sense and respond to mechanical forces in the plasma membrane, such as changes in membrane tension and curvature, and activate calcium influx (Fig. 3A) (*31*, *32*). To test this possibility, we treated zebrafish embryos with GsMTx4, an inhibitor of mechanosensitive channels, and found that apoptosis of Wnt/β-catenin–unfit cells was significantly blocked in the treated embryos (Fig. 3B). In addition, GsMTx4 treatment also blocked the translocation of Smad2 in Wnt/β-catenin–unfit cells (Fig. 3C), suggesting that the activation of mechanosensitive channels was essential for the unfit Wnt/β-catenin–triggered cell competition. To confirm the activation of mechanosensitive calcium channels, we performed live imaging of calcium ion influx using the calcium probe GCaMP7 before apoptotic elimination (Fig. 3D). As expected, the appearance of unfit cells with abnormally high or low Wnt/β-catenin activity or E-cadherin–overexpressing cells induced rapid spark-like calcium influx in the neighboring fit cells (Fig. 3, E to G, and movie S1), suggesting that abnormal Wnt/β-catenin activity and high E-cadherin levels activated calcium sparking in neighboring cells. Calcium sparks occurred most frequently in cells adjacent to unfit cells, and this frequency decreased as the distance from unfit cells increased (fig. S6A). This rapid calcium influx was blocked by GsMTx4 (Fig. 3, H and I), while GsMTx4 treatment did not affect the Wnt/β-catenin–unfit cell–driven neighboring cell movement (fig. S5, B to D). This suggested that the up-regulation of neighboring cell movement is not caused by calcium influx but is likely to occur upstream of it. We also confirmed that inhibition of apoptosis by *bcl-2* overexpression did not decrease calcium influx in neighboring cells (fig. S6B), indicating that this calcium influx is activated before the activation of apoptotic signaling. These results suggest that calcium sparks in neighboring fit cells were caused by the activation of mechanosensitive channels. Moreover, unfit cells expressing RhoACA, RhoADN, or αcatCA also induced calcium ion influx in neighboring cells (fig. S6C), suggesting that the unfit cell inducing local tension change activated mechanosensitive calcium channels. We wanted to determine which types of channels were activated because GsMTx4 selectively inhibits cation-permeable mechanosensitive channels belonging to the Piezo and transient receptor potential channel families (*33*), and the Expression Atlas (www.ebi.ac.uk/gxa/home) shows that Piezo1 is strongly expressed throughout zebrafish embryogenesis; therefore, we focused on Piezo1. Treatment with the Piezo family channel inhibitor Dooku1 blocked the elimination of unfit Wnt active cells (fig. S6D). Knockdown of the *piezo1* gene with antisense morpholinos (*piezo1* MO), which blocked the translation of the *piezo1* gene in zebrafish embryos (*34*), inhibited the activation of caspase-3 in Wnt/β-catenin–unfit cells (fig. S6E). We also generated *piezo1* knockout (KO) embryos (fig. S6, F, and G) using a triple CRISPR-Cas9 system (*35*). *piezo1* KO also blocked both the apoptotic elimination of unfit cells with abnormally high and low Wnt/β-catenin activity (fig. S6H) and calcium sparks around unfit cells

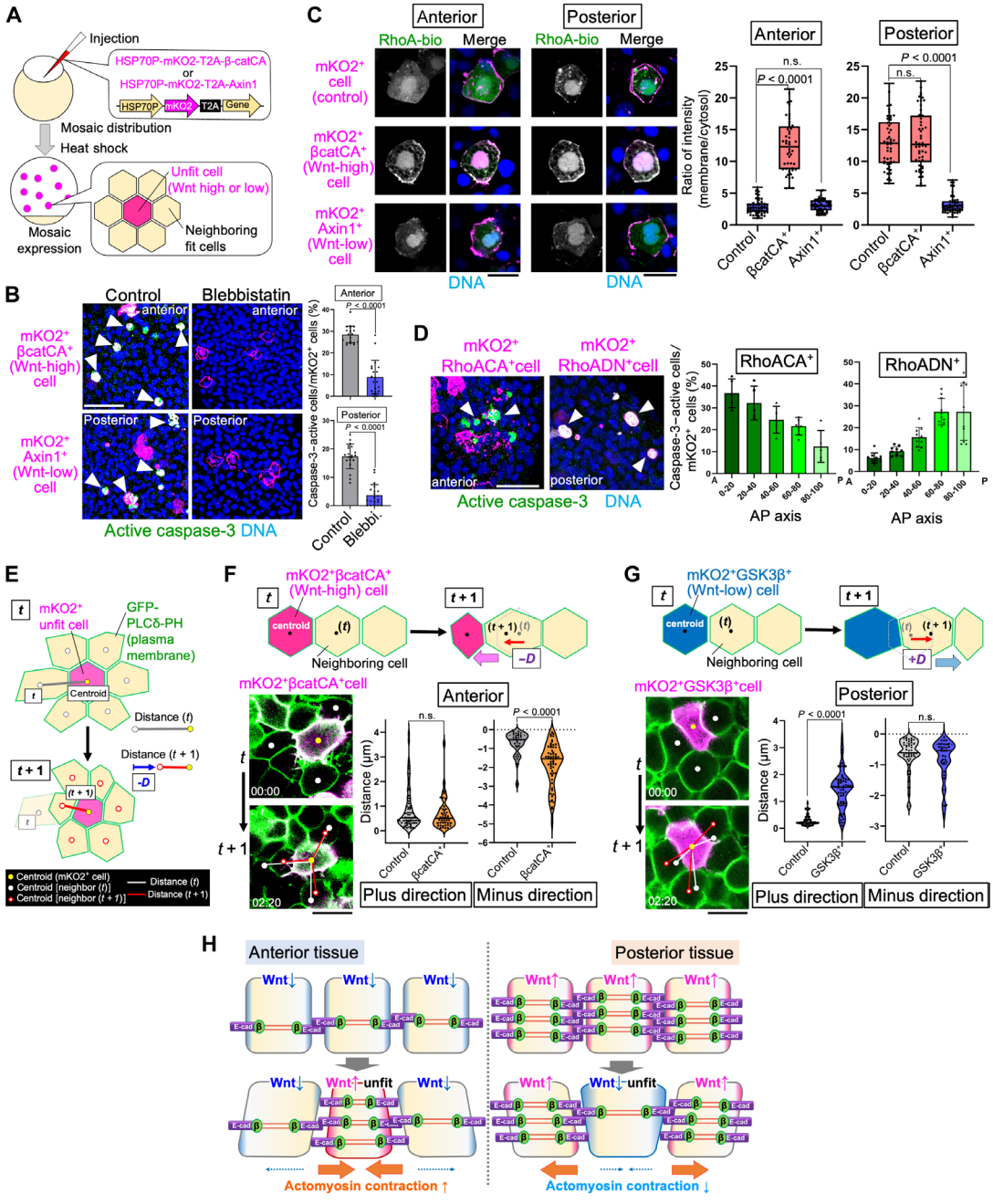

Fig. 2. Unfit Wnt/β-catenin activity generates local tension change. (**A**) Introduction of Wnt/β-catenin–unfit cells mosaically in embryos. (**B**) Active caspase-3 (green) in mosaic embryos expressing mKO2 alone (control) or with βcatCA or Axin1 (magenta) and treated with DMSO (control) or 2.5 μM blebbistatin. White arrowheads: Caspase-3–active cells. Scale bar, 50 μm. Right: Means ± SD ($n = 20$ embryos; three independent experiments) of GFP$^+$caspase-3–active cell frequencies; unpaired two-tailed t test. (**C**) Embryos injected with RhoA-biosensor mRNA (RhoA-bio, green) and mosaically introduced with mKO2$^+$ alone (control) or with βcatCA$^+$ or Axin1$^+$ cells (magenta). Right: RhoA-bio fluorescence intensities (means ± SD; $n = 50$ cells); two-tailed one-way ANOVA. Scale bars, 20 μm. (**D**) Left: Active caspase-3 (green) in mosaic embryos expressing either mKO2$^+$RhoACA$^+$ or mKO2$^+$RhoADN$^+$ (magenta). White arrowheads: Caspase-3–active cells. Scale bar, 50 μm. Right graphs: Means ± SD of caspase-3–active cell frequencies within the divided range along the AP axis of embryos mosaically expressing mKO2$^+$RhoACA$^+$ or mKO2$^+$RhoADN$^+$ ($n = 5$ embryos). (**E**) Quantification of angle and distance of neighboring cell movements. (**F** and **G**) Directions and distances of neighboring cell movements relative to βcatCA$^+$ cells in the anterior region (F) or GSK3β$^+$ cells in the posterior region (G) were quantified (top). Centroid of neighboring cell approaching unfit cells: negative direction (−D); centroid of cell that moved away: positive direction (+D). Bottom left: mKO2$^+$βcatCA$^+$ (F) or mKO2$^+$GSK3β$^+$ (G) cells (magenta). Plasma membrane (green). Lines: Distance between centroids of mKO2$^+$ (yellow spot) and neighboring cells (white spot) at time points t (white lines) and $t + 1$ (red lines). Images were acquired in the anterior region (mKO2$^+$βcatCA$^+$) or posterior region (mKO2$^+$GSK3β$^+$). Scale bar, 20 μm. Bottom right: Means ± SD ($n = 102$ cells; three independent experiments) of change in distance between the centroid of mKO2$^+$ cells and neighboring cells during 10 s, separated according to the movement direction; unpaired two-tailed t test. (**H**) Actomyosin contractile force changes around cells with abnormal Wnt/β-catenin signaling activity.

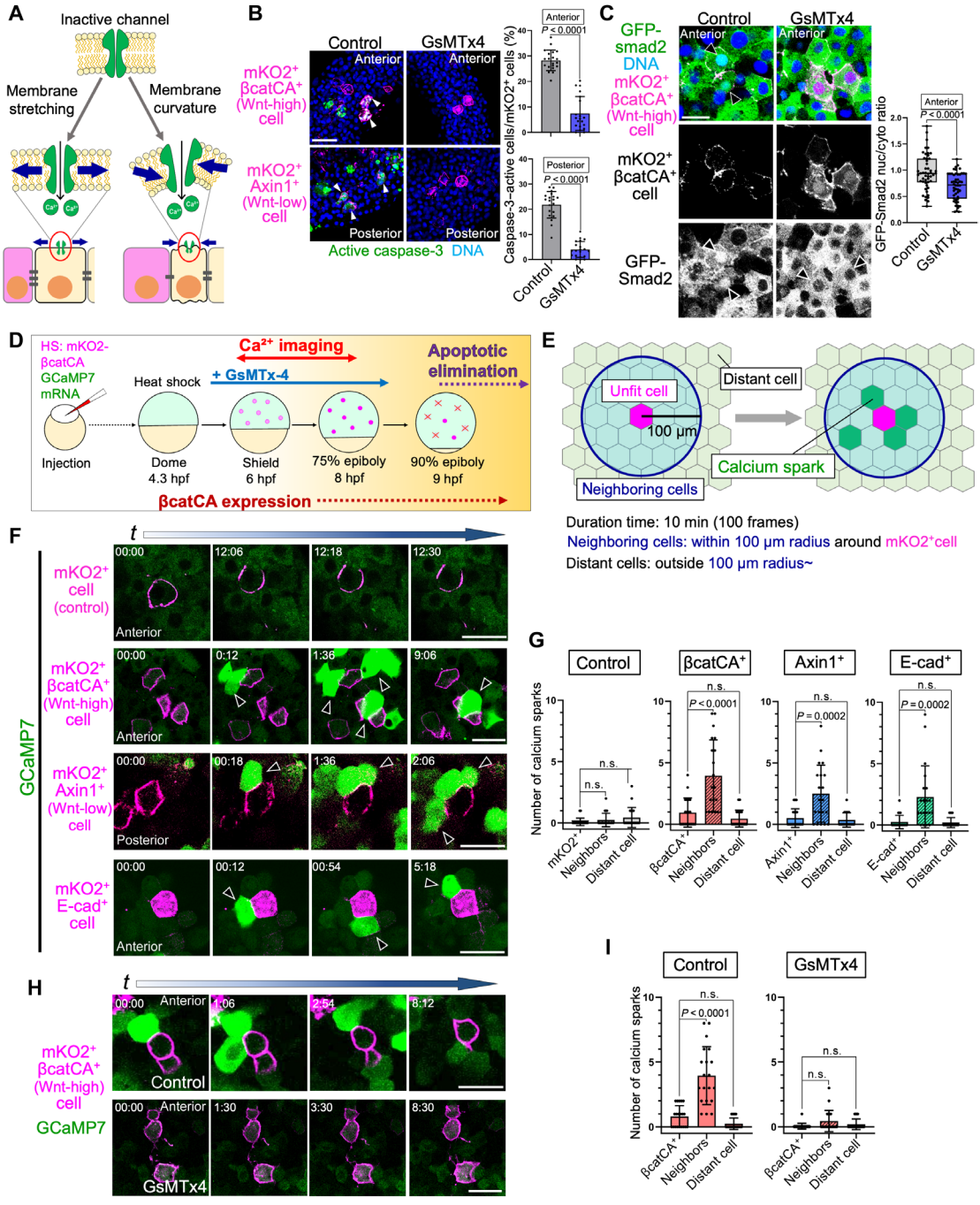

Fig. 3. Local tension change activates mechanosensitive calcium channels. (**A**) Mechanosensitive calcium channel activation by membrane stretching or curvature changes. (**B**) Active caspase-3 (green) in mosaic embryos expressing mKO2$^+$ alone (control) or with βcatCA$^+$ or Axin1$^+$ (magenta), treated with or without 2 μM GsMTx4. White arrowheads: Caspase-3–active cells. Scale bar, 50 μm. Right: Means ± SD ($n = 20$ embryos; three independent experiments) of mKO2$^+$caspase-3–active cell frequencies; unpaired two-tailed t test. (**C**) Inhibition of mechanosensitive channels blocks GFP-Smad2 translocation into unfit Wnt/β-catenin–active cell nuclei. Embryos injected with GFP-Smad2 mRNA (200 pg; green) and mosaically introduced with mKO2$^+$ alone (control) or βcatCA$^+$ cells (magenta), treated with or without 2 μM GsMTx4. Scale bar, 20 μm. Right: Nuclear/cytoplasmic GFP-Smad2 ratio. Whiskers: Minimum and maximum values. Dot: One cell (means ± SD; $n = 50$ cells; three independent experiments). Unpaired two-tailed t test. (**D**) Schematic illustration of the time course to observe calcium sparks. (**E**) Schematic illustration of quantification of calcium sparks. (**F**) Rapid calcium sparks in neighboring cells around unfit cells. mKO2$^+$ alone (control) or βcatCA$^+$, Axin1$^+$, or E-cadherin–overexpressing (E-cad$^+$; magenta) mosaic embryos were injected with GCaMP7 mRNA. The timing relative to the first image: White text. Three independent experiments. Scale bar, 50 μm. (**G**) Means ± SD ($n = 20$ embryos; three independent experiments) of the number of calcium sparks around unfit cells. All unfit cells were induced and quantified under the same conditions. Quantification: Anterior (control, βcatCA$^+$, and E-cad$^+$) or posterior (Axin1$^+$) region. Two-tailed one-way ANOVA. (**H**) mKO2$^+$βcatCA$^+$-overexpressing (magenta) mosaic embryos were injected with GCaMP7 mRNA and treated with or without 2 μM GsMTx4. The timing relative to the first image: White text. Scale bar, 50 μm. (**I**) Means ± SD ($n = 20$ embryos; three independent experiments) of the number of calcium sparks in the anterior region. Quantified under the same conditions as (G). Two-tailed one-way ANOVA.

(fig. S6I), suggesting that Piezo1 mediates calcium influx in neighboring cells to eliminate unfit cells.

Annexin A1a mediates unfit cell killing

Next, we investigated the mechanisms by which calcium influx into neighboring fit cells induces the killing of unfit cells. To identify the mediators downstream of calcium influx, we screened the genes that were up-regulated only in normal cells surrounding the unfit cells. We collected green fluorescent protein (GFP)–negative cells from embryos into which GFP-βcatCA or GFP only were mosaically introduced using the fluorescence-activated cell sorting (FACS) technique and compared the gene expression patterns using RNA sequencing (RNA-seq) (Fig. 4A) (*15*). Because secreted proteins may be involved in signaling from neighboring cells to unfit cells, we focused on secreted molecules as candidates. Among the 64 genes that were strongly up-regulated in GFP-negative cells in the embryos introduced with GFP-βcatCA cells (fig. S7A), a calcium/phospholipid-binding protein annexin A1a (ANXA1) (*36*) was the only secreted molecule that could activate Smad signaling (*37*). Using fluorescence in situ hybridization, we confirmed that ANXA1 expression was up-regulated only in normal cells neighboring unfit cells with abnormally high or low Wnt/β-catenin activities (Fig. 4, B and C, and fig. S7B). Treatment with blebbistatin or GsMTx4 blocked ANXA1 up-regulation in neighboring cells (Fig. 4, B and C, and fig. S7B), suggesting that ANXA1 was up-regulated downstream of local tension changes and mechanosensitive channel activation. Subsequently, we investigated the role of ANXA1 in unfit Wnt/β-catenin–driven cell competition. Knockdown of the *anxa1* gene with *anxa1* MO, which blocked the translation of the *anxa1* gene in zebrafish embryos (fig. S7C), inhibited the activation of Smad2 and caspase-3 in Wnt/β-catenin–unfit cells (Fig. 4, D and E). Conversely, mosaically introduced ANXA1–overexpressing cells activated Smad2 and caspase-3 in the surrounding cells (Fig. 4, F and G). Notably, mosaic ANXA1–overexpressing cells efficiently induced apoptosis to the directly adjacent cells but not to the distant cells (Fig. 4H). Inhibition of Smad activation blocked apoptosis induced by ANXA1 overexpression (fig. S7D), indicating that ANXA1 induces apoptosis via Smad activation. Overall, ANXA1 proteins secreted by neighboring cells stimulated apoptosis in surrounding cells during unfit Wnt/β-catenin–driven cell competition.

Mechanosensation and ANXA1 are required for proper patterning

Last, we examined the importance of mechanostress-induced calcium ion influx and ANXA1 activation in morphogen gradient formation and tissue patterning. GsMTx4 or *anxa1* morpholino oligonucleotide (MO) treatment induced distortion of Wnt/β-catenin gradients (Fig. 5A) and ectopic expression of brain AP markers (Fig. 5, B and C, and fig. S8A). In addition, *anxa1* MO– and GsMTx4-treated larvae displayed variable phenotypes, such as shorten-AP axis and formation of tumor-like cell mass (Fig. 5, D and E), suggesting that unfit cell elimination via mechanosensitive calcium channels and ANXA1 was required for proper formation of morphogen gradients and tissue patterns via unfit cell elimination during physiological development.

DISCUSSION

We show that the Wnt morphogen gradient is converted to a mechano-gradient, which drives cell competition–mediated elimination of unfit cells, resulting in robust patterning (Fig. 5F). During zebrafish embryonic AP pattern formation, the intercellular tension gradients (mechano-gradient) along the AP axis are formed in Wnt/β-catenin activity– and cadherin level–dependent manners. When the unfit cells produce noise in the Wnt/β-catenin morphogen gradient, this unfitness induces local deformation of the mechano-gradient, which activates mechanosensitive calcium channels and, consequently, results in the transcription of *anxa1* in neighboring fit cells. ANXA1 secreted from neighboring cells activates Smad nuclear translocation and subsequent apoptosis in unfit cells to correct the noisy Wnt morphogen gradient, thereby enabling robust patterning. Collectively, our findings indicate that chemo-mechanical and mechanochemical conversion–mediated cell competition in morphogen gradient–forming tissues ensures precise morphogen gradient formation and robust tissue patterning.

According to the general concept of morphogen-mediated patterning, individual morphogen-receiver cells obtain their positional information based on the strength of the input signal, such as "GPS," and select their fate based on the position (*38*, *39*). Here, we show that morphogen-receiver cells communicated with each other using chemical and mechanical signaling to check whether the acquired positional information was accurate and to correct the position if it was incorrect. In the Wnt/β-catenin morphogen gradient–forming tissues, Wnt/β-catenin activity changes membrane cadherin levels and generates tensile force, and, thus, adjacent cells have approximately the same levels of cadherin and tension. Therefore, in these tissues, the appearance of Wnt/β-catenin–unfit cells induces local tension changes, which are sensed by neighboring cells as mechanical stress. In other words, the morphogen gradient forms a mechano-gradient, which monitors the appearance of unfit cells that hinder proper morphogen gradient formation.

In this morphogen gradient–noise correction system, unfit cells with abnormally high and low Wnt/β-catenin activity are efficiently eliminated in the anterior and posterior tissue, respectively. However, it seems that what determines whether or not the unfit cells are eliminated is the Wnt/β-catenin activity strength in the tissue and not the positional information itself. In the anterior tissue with low Wnt/β-catenin activity, Wnt-hyperactivated cells, but not Wnt-inhibited cells, efficiently underwent apoptosis. However, in artificially Wnt/β-catenin–activated anterior tissue, Wnt-inhibited cells were efficiently removed, and Wnt-hyperactivated cells survived (fig. S8, B and C). Thus, depending on differences in signal strength, major cell populations appear to exclude minor populations as "noises."

Recent studies have suggested that cross-talk exists between chemical signaling and mechanical forces during embryogenesis (*40*–*42*). However, the association between Wnt/β-catenin signaling and mechanical force has not been well studied, although the association is predictable because β-catenin, a key molecule in canonical Wnt/β-catenin signaling, also functions as a cadherin-actomyosin linker in adherens junctions (*43*). Previously, we revealed that Wnt/β-catenin signaling abnormality is converted into membrane E-cadherin levels, which triggers activation of TGF-β–type Smads in unfit cells through communication with neighboring cells (*15*). However, in this system, Smads are activated in a TGF-β receptor–independent manner (*15*), and the mechanisms that connect the change in membrane E-cadherin and Smad activation remained unclear. In the present study, we reveal that mechano-transduction via E-cadherin–actomyosin–mechanosensitive channels mediates the Smad activation downstream of E-cadherin level changes. Our results demonstrate that the conversion of Wnt/β-catenin signaling activity into mechanical force

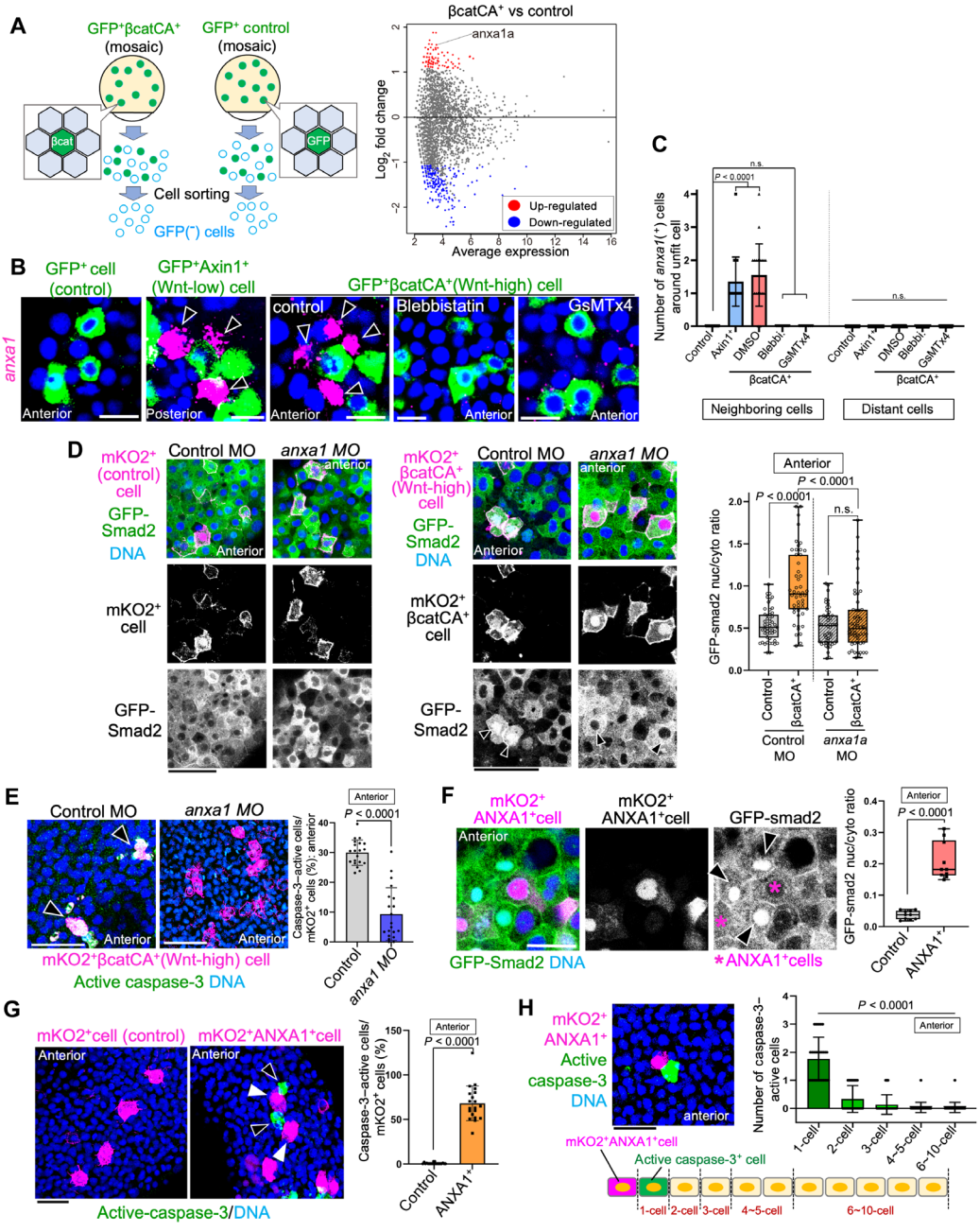

Fig. 4. ANXA1 mediates unfit cell killing. (**A**) Left: Fluorescence-activated cell sorting (FACS) of embryos. Right: Differentially expressed genes (DEGs) in GFP$^-$ cells from GFP$^+$ or GFP$^+$βcatCA$^+$-mosaic embryos. Red: Up-regulated DEGs. Blue: Down-regulated DEGs. Gray: Non-DEGs. (**B**) Endogenous *annexina1a* (*anxa1*) mRNA levels in mosaic embryos expressing mKO2$^+$alone (control) or with βcatCA$^+$ or Axin1$^+$ (magenta) and treated with DMSO (control), 2.5 μM blebbistatin, or 2 μM GsMTx4. Black arrowheads: Neighbors expressing *anxa1*. Scale bars, 50 μm. (**C**) Number of *anxa1*-expressing cells around the mKO2$^+$cells. Graph: Means ± SD (n = 20 unfit cells; three independent experiments) of *anxa1*$^{(+)}$ cells around unfit cells. Quantification: Anterior (control and βcatCA$^+$) or posterior (Axin1$^+$) region. (**D**) Embryos injected with GFP-Smad2 mRNA and mosaically introduced with mKO2$^+$ alone (control) or with βcatCA$^+$cells with control or *anxa1* morpholino oligonucleotides (MO). Scale bar, 50 μm. Black arrowheads: mKO2$^+$ cells. Right: Nuclear/cytoplasmic GFP-Smad2 ratio. Means ± SD; n = 50 cells; three independent experiments. (**E**) Active caspase-3 (green) in mosaic embryos expressing mKO2$^+$ alone (control) or with βcatCA$^+$ co-injected with control or *anxa1* MO. Black arrowheads: Caspase-3–active cells. Scale bars, 50 μm. Right: Means ± SD (n = 20 embryos; three independent experiments) of mKO2$^+$caspase-3–active cell frequencies. (**F**) Cells expressing mKO2$^+$ annexin A1 (ANXA1$^+$) in GFP-Smad2 mRNA–injected embryos. Scale bar, 50 μm. Right: Nuclear/cytoplasmic ratio of GFP-Smad2 intensity in neighboring cells around mKO2$^+$ alone (control) and ANXA1$^+$ cells. n = 10 embryos from three independent experiments. (**G**) Embryos mosaically transfected with mKO2$^+$ alone (control) or with ANXA1$^+$ cells. White arrowheads: ANXA1$^+$ cells. Black arrowheads: Caspase-3–active cells. Scale bar, 50 μm. Right: Means ± SD (n = 20 embryos; three independent experiments) of mKO2$^+$caspase-3–active cell frequencies. Unpaired two-tailed t test. (**H**) Left: Active caspase-3 around mKO2$^+$ANXA1$^+$ cells induced very few numbers. Right: Means ± SD (n = 20 ANXA1$^+$ cells; three independent experiments) of the number of mKO2$^+$caspase-3–active cells around ANXA1$^+$ cells according to the distance from ANXA1$^+$ cells. [(C) to (F) and (H)] Two-tailed one-way ANOVA.

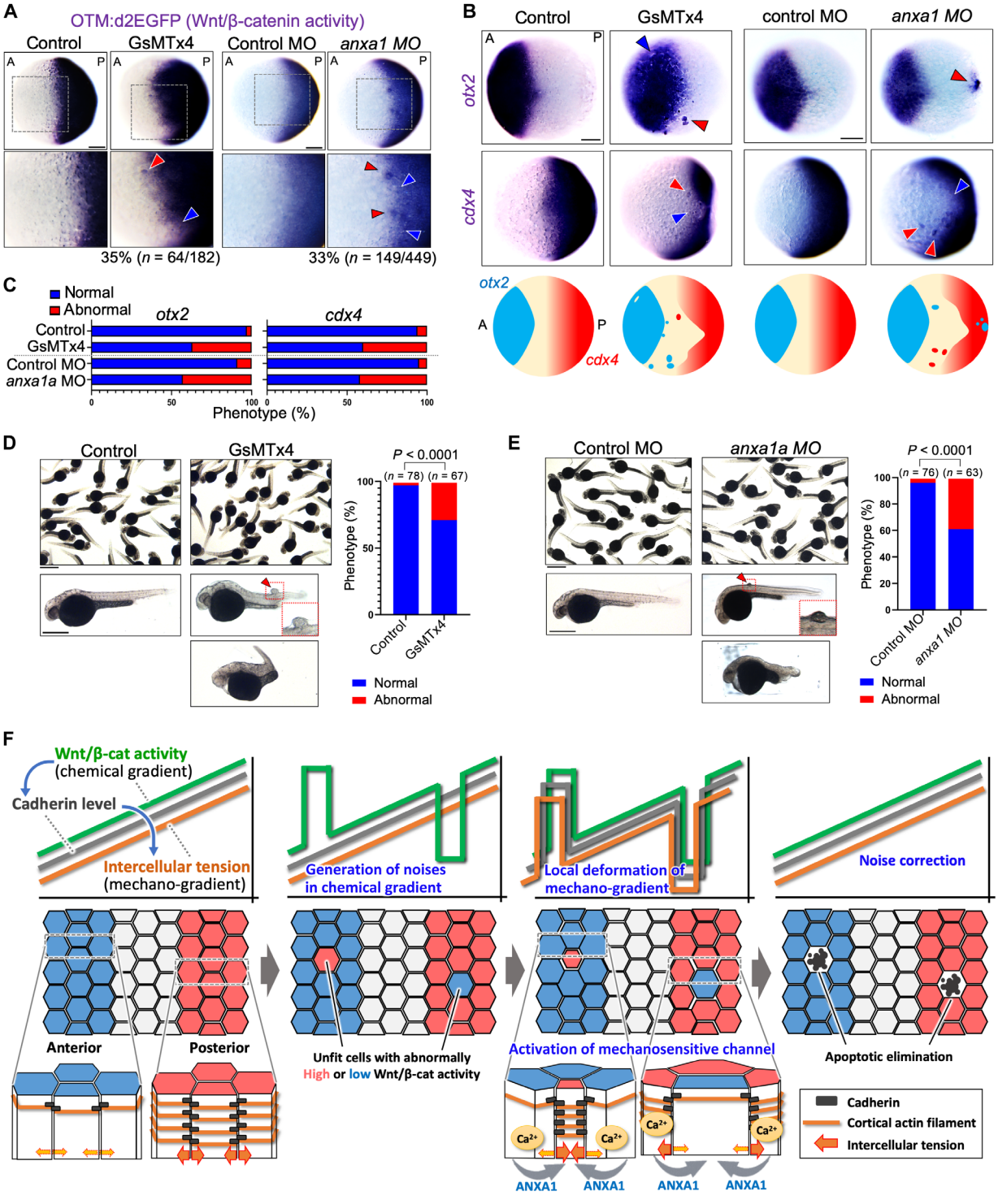

Fig. 5. Chemo-mechanical interconversion–driven cell competition ensures robust formation of morphogen gradients. (**A**) d2EGFP in Tg (OTM:d2EGFP) embryos (dorsal view) treated with or without 2 μM GsMTx4 (left) and injected with control or *anxa1* MO (right). Red arrowheads: Abnormally high Wnt/β-catenin activity. Blue arrowheads: Abnormally low Wnt/β-catenin activity. Scale bars, 200 μm. (**B**) *otx2* and *cdx4* expression in embryos treated with or without 2 μM GsMTx4 (left) and injected with control MO or *anxa1a* MO (right). Scale bars, 200 μm. Bottom: Brain AP marker expression patterns. (**C**) Percentage of embryos with normal or abnormal expression patterns. (**D** and **E**) GsMTx4 treatment or *anxa1a* KD induces abnormal morphogenesis. Images show 32-hpf zebrafish larvae treated with or without 2 μM GsMTx4 from 6 to 9 hpf (D) or injected with control MO or *anxa1a* MO (E). Red arrow indicates abnormal cell proliferation. Scale bars, 500 μm. Percentages of embryos with normal or abnormal morphology are shown in the graph on the right. The numbers shown above the graph indicate the total number of embryos analyzed (Fisher's exact test). (**F**) Mechano-gradient–mediated correction of noisy morphogen gradients.

via cadherin and actomyosin is important for the proper formation of the Wnt/β-catenin morphogen gradient and brain AP pattern. Because the Wnt/β-catenin morphogen gradient is formed in a variety of developing and regenerating tissues and a recent study showed that Shh morphogen signaling activity regulates the expression levels of cadherin family proteins in zebrafish spinal cord patterning (*44*), this chemo-mechanical conversion–mediated cell competition may support not only embryonic AP patterning but may also contribute to morphogen-mediated embryonic tissue patterning and adult tissue homeostasis.

Although a variety of genetic and chemical signaling abnormalities that trigger cell competition have been reported, how these signal abnormalities are sensed by neighboring fit cells and how they trigger a common mechanism of elimination of abnormal cells remain unclear. Particularly in the cell competition system that corrects morphogen gradients, the appearance of both abnormally high and low Wnt/β-catenin–unfit cells activates Smad signaling in unfit cells via communication between the unfit and neighboring cells (*15*). From the viewpoint of chemical signal transduction, interpreting how opposite chemical signals activate the same downstream pathways is challenging. In this study, from a mechanical signaling perspective, we demonstrate that opposite chemical signals (unfit activation and inhibition of Wnt/β-catenin signaling) cause mechanical stress on neighboring cells, thereby initiating cell competition. Although recent studies have reported that mechanical stress acts as a driver of cell competition (*45*, *46*), the involvement of mechanical force in sensing unfit cells with defective chemical signaling is poorly understood. Our discovery that chemo-mechanical and mechanochemical conversions drive cell competition provides a previously unidentified concept for understanding the mechanisms of cell competition.

We show here that the gradient of actomyosin contractile force, named mechano-gradient, is formed along the AP axis in zebrafish embryos. Treatment with a low concentration (2.5 μM) of blebbistatin revealed that the mechano-gradient contributes to the error correction of the morphogen gradient. However, a concentration of 2.5 μM is much lower than the typical concentration of blebbistatin used for zebrafish (10 μM) (*47*, *48*), suggesting that minor changes in actomyosin contractile force are sufficient to initiate cell competition–mediated unfit cell elimination. Besides unfit cell elimination, mechano-gradients may have other functions. Treatment with blebbistatin at 10 μM inhibited gastrulation (fig. S1B), and previous studies reported that the actomyosin system plays important roles in zebrafish gastrulation (*23*, *49*, *50*). Because the mechano-gradient is formed during the gastrulation stage and cells collectively migrate to the posterior region during this process, the mechano-gradient might be used as the driving force for gastrulation. Although we succeeded in partially elucidating the significance of the mechano-gradient, this gradient may play other unknown roles. Elucidation of these roles in the future will enhance our understanding of mechanical control and mechanochemical cross-talk during tissue development and regeneration.

Mechanosensitive calcium ion channels sense the mechanical forces applied to the plasma membrane and convert them into chemical signals via calcium ion influx. We show that the mechanosensitive calcium channels, especially the Piezo family channels, are involved in unfit Wnt/β-catenin–driven cell competition. However, it remains unclear how the Piezo channel is activated only in neighboring cells but not in the unfit cells due to the imbalance of contractility. It has been reported that mechanosensitive channels are efficiently activated by asymmetric forces applied to the plasma membrane, such as membrane curvature and stretching (*51*, *52*). In the process of Wnt/β-catenin–driven cell competition, the contractile activity increases in Wnt-hyperactivated cells, and a decrease in Wnt-inhibited cells would induce membrane stretching and curvature, respectively, in neighboring fit cells, and, consequently, they would activate mechanosensitive channels. Notably, Wnt/β-catenin–unfit cells moved smoothly in the same direction as the collective cell movement during gastrulation, while the trajectories of the neighboring fit cells were very wavy (fig. S9, A and B). This wavy movement of neighbors might be induced by the unfit cells' contraction or relaxation owing to the changes in the abnormal Wnt signaling–driven actomyosin contractile force. These different movements might explain, in part, why the Piezo channel is activated specifically in neighbors but not unfit cells. However, further studies are needed to identify the detailed mechanisms of how the force direction and membrane stretching/deformation affect the activity of the Piezo channel in neighbors. In addition, the detailed mechanisms by which calcium channels activate ANXA1 expression require further investigation. One candidate mediator is calcium/calmodulin-dependent protein kinase II (CaMKII) because the transcription factor cyclic adenosine 3′,5′-monophosphate response element–binding protein (CREB), which acts downstream of CaMKII, regulates ANXA1 expression (*53*). In addition, treatment with the CaMKII inhibitor, KN-93, suppressed the activation of Smad and caspase-3 in Wnt/β-catenin–unfit cells (fig. S9, C and D), suggesting that ANXA1 expression may be up-regulated downstream of CaMKII. ANXA1 was previously reported to enhance TGF-β/Smad signaling (*37*). Here, ANXA1 produced in neighboring cells stimulates TGF-β–type Smad signaling in Wnt/β-catenin–unfit cells and causes unfit cell apoptosis. How the secreted ANXA1 targets unfit cells and induces apoptosis remains unclear. Because ANXA1 binds to phospholipid membranes in a $Ca2^{+}$-dependent manner, ANXA1 may recognize changes in membrane components, such as lipids, in unfit cells. However, the detailed mechanism by which ANXA1 selectively kills unfit cells requires further investigation. In addition, the detailed mechanism of how ANXA1-expressing cells activate Smad signaling, specifically in unfit cells but not in themselves, needs to be delineated. Our previous report showed that a negative regulator of Smad, *skilb*, is specifically down-regulated in Wnt/β-catenin–unfit cells but not in neighboring cells and that *skilb* overexpression blocks unfit cells (*15*). The unfit cells may make them more susceptible to Smad activation by reducing *skilb* expression.

Unfit cells with an abnormally active Wnt signaling pathway represent the origin of cancer (*54*, *55*). When Wnt signaling–hyperactivated cells were mosaically introduced into the mouse intestine, they up-regulated E-cadherin expression and underwent apoptosis (*56*). E-cadherin and Smad2/4 are known as tumor suppressors (*57*, *58*). ANXA1 is also a tumor suppressor that induces cancer cell apoptosis (*36*, *59*, *60*). Therefore, the morphogen gradient–correcting cell competition mediated by cadherin, ANXA1, and Smad, which was discovered in this study, may also be present in tissues where homeostatic Wnt/β-catenin gradients are maintained, such as the intestinal crypt and work as a mechanical force–mediated defense system against cancer.

Overall, we have shown that mechano-gradients drive cell competition–mediated morphogen-noise correction. In conclusion, our findings provide previously unidentified insights into intercellular

communication mechanisms that orchestrate chemical morphogen gradients and mechanical interactions to maintain robust patterning. The role of the mechano-gradient in mechanochemical crosstalk during tissue development and regeneration should be further elucidated in future studies.

MATERIALS AND METHODS

Ethical approval

All experiments with animals were performed according to institutional and national guidelines and regulations. The study protocol was approved by the Institutional Animal Care and Use Committee of Osaka University (RIMD permit no. Biken-AP-R02-04). This study was conducted in accordance with the ARRIVE (Animal Research: Reporting of In Vivo Experiments) guidelines.

Zebrafish maintenance

Zebrafish were raised and maintained under standard conditions. Wild-type strains (AB) were used, along with the following transgenic lines: Tg (OTM:d2EGFP) (*61*), Tg (OTM:ELuc-CP), Tg (hsp70l:GFP–T2A–βcatCA), and Tg (HS:dkk1b-GFP) (*62*). One-cell-stage embryos were used for cell injection to generate transgenic fish or mosaic embryos, with mosaic embryos being processed up to 9 hours postfertilization (hpf). One- and two-cell-stage embryos were used for mRNA and MO injections, respectively. Alternatively, cells were injected into 3.3- to 3.7-hpf stage embryos.

Plasmids

To prepare heat-shock promoter–driven plasmids, the hsp70l promoter was subcloned into the pTol2 vector (a gift from K. Kawakami). Subsequently, membrane-tagged (GAP43-fused) GFP (or mKO2) and T2A were subcloned into the pTol2-hsp70l promoter plasmid. These plasmids expressed only membrane-specific GFP (or mKO2) in response to heat shock. N terminus–truncated mouse β-catenin (βcatCA) (*63*) was used as a Wnt/β-catenin signaling activator. Human wild-type GSK3β (a gift from A. Kikuchi) and rat Axin1 were used as Wnt/β-catenin signaling inhibitors. The plasmids were used in our previous study (*15*). Other signaling regulators were as follows: human ANXA1-GFP (a gift from V. Gerke and U. Rescher; Addgene, catalog no. 107194) (*64*), EGFP-RhoA-Q63L (a gift from G. Bokoch; Addgene, catalog no. 12968) (*65*), RhoA-T19N (a gift from G. Bokoch; Addgene, catalog no. 12963), and α-catenin M319G/R326E (a gift from J. Ikenouchi) (*28*). Cloned signaling proteins were as follows: human Bcl-2 (a gift from S. Korsmeyer; Addgene, catalog no. 8768) (*66*), zebrafish E-cadherin–GFP fusion gene (a gift from E. Raz) (*67*), zebrafish dkk1b (a gift from M. Hibi) (*68*), pCS2-GCaMP7 (a gift from J. Nakai), and GFP-fusion zebrafish Smad24. For visualizing RhoA activity, GFP-RhoA biosensor (a gift from M. Glotzer; Addgene, catalog no. 68026) (*22*) was used. For visualizing plasma membrane and F-actin, GFP-PLCδ-PH (a gift from T. Meyer; Addgene. catalog no. 21179) (*69*) and Lifeact-Ruby (a gift from M. Tada) were used. L344P point mutation was introduced into the α-catenin M319G/R326E gene using a QuikChange Site-Directed Mutagenesis kit (Agilent, Santa Clara, CA).

Mosaic introduction of unfit cells

Hsp70 promoter–driven plasmids (5 to 17.5 pg) were injected into one-cell-stage embryos and maintained at 28.5°C until 4.3 hpf (dome stage). At 4.3 hpf, the embryos were exposed to heat shock. Briefly, embryos were transferred to pre-warmed egg water at 37°C and kept at 37°C for 1 hour. After heat shock, embryos were placed at 28.5°C and then fixed at 9 hpf for immunostaining or in situ hybridization. This method allowed the introduction of unfit cells at the single-cell level but not at the patchy-clone level.

Quantification of membrane E-cadherin, cortical F-actin, and RhoA activity levels

Fluorescence intensity in two intercellular areas per cell ($n = 6$ cells) in each region was measured. All analyses were performed in duplicates.

Antibodies

Primary antibodies were as follows: anti–β-catenin (catalog no. C7207, Sigma-Aldrich; 1:500), anti–E-cadherin (catalog no. 610181, BD Biosciences, Franklin Lakes, NJ, USA; 1:200 dilution for immunofluorescence), mouse anti-GFP (catalog no. A-11120, Thermo Fisher Scientific, Waltham, MA, USA; 1:100), anti–phospho-MLC2 (Thr^{18}/Ser^{19}; catalog no. 95777S, Cell Signaling Technology, Mountain View, CA, USA; 1:300), anti–active-caspase3 (catalog no. 9661, Cell Signaling Technology; 1:500), and anti-mKO2 (catalog no. M168-3 M, MBL, Nagoya, Japan; 1:500). Secondary antibodies were as follows: Alexa Fluor 488–conjugated anti-mouse immunoglobulin G (IgG; catalog no. A-11029, Invitrogen, Waltham, MA, USA; 1:300) and anti-rabbit IgG (catalog no. A-11034, Invitrogen; 1:300), Alexa Fluor 594–conjugated anti-mouse IgG (catalog no. A-11032, Invitrogen; 1:300) and anti-rabbit IgG (catalog no. A-11037, Invitrogen; 1:300), and Alexa Fluor 647–conjugated anti-rabbit IgG (catalog no. 4414, Cell Signaling Technology; 1:500). For F-actin staining, phalloidins AF-488 (catalog no. A12379, Invitrogen; 1:400) and AF647 (catalog no. A22287, Invitrogen; 1:400) were used as secondary antibodies.

mRNA and antisense MO microinjection

Capped mRNA was synthesized using the SP6 mMessage mMachine kit (Ambion, Austin, TX, USA) and purified using Micro Bio-Spin columns (Bio-Rad, Hercules, CA, USA). We injected the synthesized mRNA into zebrafish embryos at the one-cell stage. To perform knockdown experiments on zebrafish embryos, antisense MOs (Gene Tools, Philomath, OR, USA) were injected into one- and/or two-cell-stage embryos. Standard control MO: 5′-CCTCTTACCTCAGTTACAATTTATA-3′;*E-cadherin*(*cdh1*):5′-AAAGTCTTACCTGAAAAAGAAAAAC-3′ (*70*) (0.3 ng); *piezo1* MO: 5′-AATATGCAGGCTGTGGAAAACACAT-3′ (*34*) (10 ng); and *annexina1a* (*anxa1*) MO: 5′-CACACC TGAGAGCAAAATTGACTGT-3′ (10 ng) were used.

Chemical inhibitors

The myosin inhibitor blebbistatin (FUJIFILM Wako, Osaka, Japan), ROCK inhibitor Y27632 (FUJIFILM Wako), RhoA activator II CN03 (Cytoskeleton Inc., CO, USA), mechanosensitive channels inhibitor GsMTx4 (TOCRIS, Bristol, UK), piezo channel inhibitor Dooku1 (MedChemExpress, NJ, USA), and CaMKII inhibitor KN-93 (Tokyo Chemical Industry, Tokyo, Japan) were used.

Whole-mount immunostaining

Embryos were fixed with 4% paraformaldehyde in phosphate-buffered saline (PBS) overnight at 4°C. The dechorionated embryos were washed with 0.5% Triton X-100 (PBST) four times and blocked with 10% fetal bovine serum, 4% Block Ace (Megmilk Snow Brand, Tokyo, Japan), and

1% dimethyl sulfoxide (DMSO) in 0.1% PBST for 1 hour. The embryos were incubated with the primary antibodies overnight at 4°C and then washed and incubated with Alexa Fluor–conjugated secondary antibodies and Hoechst 33342 (Invitrogen, H3570) overnight at 4°C. Stained embryos were visualized using an M205FA fluorescence stereomicroscope (Leica, Wetzlar, Germany) or an FV3000 (EVIDENT, Tokyo, Japan) confocal laser-scanning microscope. Images were prepared and analyzed using ImageJ (https://imagej.net/ij/) software. To quantify the membrane E-cadherin, F-actin, and P-MLC2 levels, the fluorescence intensity in two intercellular areas per cell ($n = 5$) in each region was measured. All analyses were performed in duplicates.

Time-lapse imaging of calcium ion influx and cell movements

For time-lapse confocal live imaging of calcium influx, GCaMP7 mRNA (200 pg) and pT2 HSP70P mKO2–T2A–β-catenin CA, Axin1, or E-cadherin DNA (25 pg) were co-injected into the yolk of one-cell-stage embryos. For quantification of cell movements, GFP-PLCδ-PH mRNA (200 pg), pT2 HSP70P mKO2–T2A–β-catenin CA, or GSK3β DNA (25 pg) was co-injected. Embryos were manually dechorionated using forceps and mounted in 1% low-melting agarose with egg water onto glass bottom dishes. Live imaging was performed in the deep cell region using an FV3000 confocal laser-scanning microscope (EVIDENT). Two laser lines at 488 and 594 nm were used. The recording interval was 6 s (for calcium ion imaging) or 10 s (for cell movement imaging), and recording was performed for 10 min.

Quantification of cell movements

For quantification of the angles of neighboring cell movements relative to the unfit cells, positions of the centroids of $mKO2^{+}\beta catCA^{+}$ or $mKO2^{+}GSK3\beta^{+}$ (unfit) cells and neighboring cells at each time point were detected on the basis of the plasma membrane marker GFP-PLCδ-PH using ImageJ. Neighboring cells around $\beta catCA^{+}$ (Wnt-hyperactivated) cells in the anterior region or $GSK3\beta^{+}$ (Wnt-inhibited) cells in the posterior region were quantified. The movement angle was measured between the movement vector of the neighboring cell and a vector pointing toward the centroid of the unfit cell (unfit cell direction vector). At each time point, the movement angles were calculated and plotted as histograms. An angle of 0° represents neighboring cell movement in parallel with the unfit cell. The measurement was performed every 6 s (1 frame), and the total duration was 10 min (100 frames).

To quantify the direction and distance of neighboring cell movements relative to the unfit cells, the positions of the centroids of the unfit and neighboring cells at each time point were detected in a similar manner. At each time point, the distance between the centroid of the unfit cell and the neighboring cell was measured using ImageJ software. The change in distance between the unfit cell and the neighboring cell from the previous time point was measured as the "movement distance" of neighboring cells during 6 s (1 frame). The total duration of measurement was 10 min (100 frames). The movement distance of neighboring cells approaching the unfit cells was considered as the negative (minus) direction, and the movement distance of cells moving away from the unfit cells was considered as the positive (plus) direction.

The tracking analysis of unfit cells and neighboring cells was performed using images taken under the same conditions as above. For quantification of changes in the movement direction, we counted the number of turns in the trajectory below 120° from the previous time point. The total duration of measurement was 180 s (30 frames).

Quantification of calcium influx

For quantification of calcium influx frequency, we defined deep cells within a 100 μm radius around the abnormal cell labeled with mKO2 as a group of "neighboring fit cells." For each cell within this range, we counted cells that showed a temporary increase in fluorescence intensity by 50% or more from the previous frame and a decrease within 40 frames as a calcium spark. The cells outside this range were counted as "distant cells." The total duration of measurement was 10 min (100 frames, 6 s per frame). For the quantification of calcium spark according to distance from abnormal cells, we defined neighboring fit cells (one cell) within a 33 μm radius around the abnormal cell labeled with mKO2, neighboring fit cells (two cells) within a 66 μm radius, and neighboring fit cells (three cells) within a 100 μm radius. Cells outside the 100 μm radius were defined as distant cells. The total duration of measurement was 10 min (100 frames, 6 s per frame).

Laser dissection

The mKO2-Lifeact mRNA (200 pg) was injected into the embryos. After incubation, 8 hpf embryos (80 to 90% epiboly) were embedded in low-melting point agarose gel and observed using a confocal microscope. Subsequently, linear regions of interest were set for the three target cells, and laser-scanning microscopy stimulation was performed by irradiating them at 405-nm wavelength and 100% intensity for 120 s at 2 μs/pixel. Immediately after this, time-lapse imaging was performed for 80 cycles at 6 s per frame. The longest width of the laser wound was measured using ImageJ and plotted as the maximum recoil distance (micrometers).

Triple-target CRISPR

To perform knockout experiments on zebrafish embryos using the CRISPR-Cas9 system, we performed a triple-target CRISPR protocol based on a previously reported method (*35*). We selected three single-guide RNA (sgRNA) targeting sites on the protein-coding sequences for exon 3 of the *piezo1* gene, aiming to induce frameshift mutation using the chop-chop program. sgRNA target site was selected as follows: control sgRNAs: DsRed2#1, GGCCACGAGTTCGAGATCGAGGG;DsRed2#2,CTCGGTGATGACGTTCTCGGAGG; and DsRed2#3, GGAGCCGTACTGGAACTGGGGGG; and *piezo1* sgRNAs: *piezo1*#1, TGCGTCATCAAGGCTTGGGATGG; *piezo1*#2, CCCAGTGCGTCATCAAGGCTTGG; and *piezo1*#3, CAAGGCTTGGGATGGTATACAGG.

sgRNAs were synthesized and purified using the CUGA 7 in vitro Transcription Kit (NIPPON GENE, Tokyo, Japan). We injected synthesized sgRNAs at the one-cell stage of zebrafish embryos. An injection solution was prepared as follows: 20 ng/μl for each sgRNA, 1 μM Cas9 Protein (New England Biolabs), and 20% Phenol Red (Sigma). For each embryo, 2 nl of solution was injected and examined at the 6- to 8-hpf stage of the embryo.

RNA-seq analysis

Data were collected simultaneously as in a previous study (*15*). βcatCA–mosaically introduced embryos were prepared, and, then, cell dissociation was performed as previously described. $\beta catCA^{+}GFP^{+}$ cells and GFP^{-} cells were sorted by FACSAriaII (BD Biosciences). Control embryos expressing only GFP were sorted under the same

conditions. The sorted cells were pelleted and dissolved in TRIzol reagent (Invitrogen). Libraries were constructed following a published protocol (*71*) and sequenced using Illumina HiSeq 1500 (Illumina, San Diego, CA, USA). The reads were aligned to the zebrafish reference genome (GRCz10) using Bowtie2 software (version 2.3.1) (*72*). Read counting was performed per gene with HTSeq (version 0.6.1) (*73*), and duplicates in unique molecular identifiers were discarded. Differentially expressed genes were extracted using the resulting counts, and the $\log_2$ fold change versus average expression was plotted using iDEP 0.96 (*74*). The RNA-seq data have been deposited in the National Center for Biotechnology Information Gene Expression Omnibus (GEO) database under the accession code GSE254439.

Whole-mount in situ hybridization

RNA probe synthesis was performed as previously described (*75*). The probes used were *annexina1a* (*anxa1*), *otx2*, *cdx4*, and *Emerald luciferase* (*ELuc*). Whole-mount in situ hybridization and fluorescence in situ hybridization were performed as previously described (*75*, *76*). Digoxigenin- or fluorescein isothiocyanate–labeled RNA antisense probes were prepared from plasmids containing *anxa1*, *otx2*, *cdx4*, and *Eluc*. Images were obtained using an FV3000 confocal laser-scanning microscope.

Measurement of the area of abnormal pattern formation

The in situ hybridization images of Wnt/β-catenin reporter (OTM: d2EGFP) and *otx2* and *cdx4* marker expression were binarized using "MaxEntropy Threshold Image Filter" in ImageJ. For binarization, we used min (136) and max (255) to define the threshold. Using binarized images, we quantified the ectopically activated/expressed area and ectopically reduced area in each embryo using ImageJ and plotted the total area from one embryo.

Statistical analysis

Embryos without severe morphological defects were selected for imaging. Differences between groups were examined using two-tailed unpaired Student's *t* test, one-way analysis of variance (ANOVA), and the chi-square test using Prism 8 (GraphPad Software, San Diego, CA, USA) or Excel (Microsoft, Redmond, WA, USA). Statistical significance was set at $P < 0.05$. Representative images or plots were obtained from at least two independent experiments.

Supplementary Materials

The PDF file includes:
Figs. S1 to S9
Legend for movie S1
Legends for supplementary Excel files 1 to 3
Full scan image of fig. S6F

Other Supplementary Material for this manuscript includes the following:
Movie S1
Supplementary Excel files 1 to 3

REFERENCES AND NOTES

1. A. Turing, The chemical basis of morphogenesis. *Phil. Trans. R. Soc. Lond. B* **237**, 37–72 (1952).
2. L. Wolpert, Positional information and the spatial pattern of cellular differentiationt. *J. Theor. Biol.* **25**, 1–47 (1969).
3. A. F. Schier, W. S. Talbot, Molecular genetics of axis formation in zebrafish. *Annu. Rev. Genet.* **39**, 561–613 (2005).
4. J. Howard, S. W. Grill, J. S. Bois, Turing's next steps: The mechanochemical basis of morphogenesis. *Nat. Rev. Mol. Cell Biol.* **12**, 392–398 (2011).
5. C. P. Heisenberg, Y. Bellaïche, Forces in tissue morphogenesis and patterning. *Cell* **153**, 948–962 (2013).
6. K. Dasbiswas, E. Hannezo, N. S. Gov, Theory of epithelial cell shape transitions induced by Mechanoactive chemical gradients. *Biophys. J.* **114**, 968–977 (2018).
7. M. Murrell, P. W. Oakes, M. Lenz, M. L. Gardel, Forcing cells into shape: The mechanics of actomyosin contractility. *Nat. Rev. Mol. Cell Biol.* **11**, 337–343 (2015).
8. C. T. Mierke, Viscoelasticity, like forces, plays a role in mechanotransduction. *Front. Cell Dev. Biol.* **10**, 789841 (2022).
9. Q. Yang, S. L. Xue, C. J. Chan, M. Rempfler, D. Vischi, F. Maurer-Gutierrez, T. Hiiragi, E. Hannezo, P. Liberali, Cell fate coordinates mechano-osmotic forces in intestinal crypt formation. *Nat. Cell Biol.* **23**, 733–744 (2021).
10. R. Priya, S. Allanki, A. Gentile, S. Mansingh, V. Uribe, H. M. Maischein, D. Y. R. Stainier, Tension heterogeneity directs form and fate to pattern the myocardial wall. *Nature* **588**, 130–134 (2020).
11. J. P. McMurrich, in *On Growth and Form* (Cambridge University Press, 1917), vol. 8, p. 779.
12. K. W. Rogers, A. F. Schier, Morphogen gradients: From generation to interpretation. *Annu. Rev. Cell Dev. Biol.* **27**, 377–407 (2011).
13. A. Sagner, J. Briscoe, Morphogen interpretation: Concentration, time, competence, and signalling dynamics. *Wiley Interdiscip. Rev. Dev. Biol.* **6**, e271 (2017).
14. K. S. Stapornwongkul, J. P. Vincent, Generation of extracellular morphogen gradients: The case for diffusion. *Nat. Rev. Genet.* **22**, 393–411 (2021).
15. Y. Akieda, S. Ogamino, H. Furuie, S. Ishitani, R. Akiyoshi, J. Nogami, T. Masuda, N. Shimizu, Y. Ohkawa, T. Ishitani, Cell competition corrects noisy Wnt morphogen gradients to achieve robust patterning in the zebrafish embryo. *Nat. Commun.* **10**, 4710 (2019).
16. G. A. Gomez, R. W. McLachlan, A. S. Yap, Productive tension: Force-sensing and homeostasis of cell-cell junctions. *Trends Cell Biol.* **21**, 499–505 (2011).
17. N. Borghi, M. Sorokina, O. G. Shcherbakova, W. I. Weis, B. L. Pruitt, W. J. Nelson, A. R. Dunn, E-cadherin is under constitutive actomyosin-generated tension that is increased at cell-cell contacts upon externally applied stretch. *Proc. Natl. Acad. Sci. U.S.A.* **109**, 12568–12573 (2012).
18. C. D. Buckley, J. Tan, K. L. Anderson, D. Hanein, N. Volkmann, W. I. Weis, W. J. Nelson, A. R. Dunn, Cell adhesion. The minimal cadherin-catenin complex binds to actin filaments under force. *Science* **346**, 1254211 (2014).
19. C. Pérez-González, R. Alert, C. Blanch-Mercader, M. Gómez-González, T. Kolodziej, E. Bazellieres, J. Casademunt, X. Trepat, Active wetting of epithelial tissues. *Nat. Phys.* **15**, 79–88 (2019).
20. M. Amano, M. Nakayama, K. Kaibuchi, Rho-kinase/ROCK: A key regulator of the cytoskeleton and cell polarity. *Cytoskeleton* **67**, 545–554 (2010).
21. R. J. Marjoram, E. C. Lessey, K. Burridge, Regulation of RhoA activity by adhesion molecules and mechanotransduction. *Curr. Mol. Med.* **14**, 199–208 (2014).
22. A. J. Piekny, M. Glotzer, Anillin is a scaffold protein that links RhoA, actin, and myosin during cytokinesis. *Curr. Biol.* **18**, 30–36 (2008).
23. M. Behrndt, G. Salbreux, P. Campinho, R. Hauschild, F. Oswald, J. Roensch, S. W. Grill, C. P. Heisenberg, Forces driving epithelial spreading in zebrafish gastrulation. *Science* **338**, 257–260 (2012).
24. L. Carvalho, C. P. Heisenberg, The yolk syncytial layer in early zebrafish development. *Trends Cell Biol.* **20**, 586–592 (2010).
25. S. Yonemura, Y. Wada, T. Watanabe, A. Nagafuchi, M. Shibata, α-catenin as a tension transducer that induces adherens junction development. *Nat. Cell Biol.* **12**, 533–542 (2010).
26. N. Ishiyama, N. Tanaka, K. Abe, Y. J. Yang, Y. M. Abbas, M. Umitsu, B. Nagar, S. A. Bueler, J. L. Rubinstein, M. Takeichi, M. Ikura, An autoinhibited structure of α-catenin and its implications for vinculin recruitment to adherens junctions. *J. Biol. Chem.* **288**, 15913–15925 (2013).
27. K. Maki, S. W. Han, Y. Hirano, S. Yonemura, T. Hakoshima, T. Adachi, Mechano-adaptive sensory mechanism of α-catenin under tension. *Sci. Rep.* **6**, 24878 (2016).
28. K. Matsuzawa, T. Himoto, Y. Mochizuki, J. Ikenouchi, α-Catenin controls the anisotropy of force distribution at cell-cell junctions during collective cell migration. *Cell Rep.* **23**, 3447–3456 (2018).
29. X. Peng, J. L. Maiers, D. Choudhury, S. W. Craig, K. A. DeMali, α-Catenin uses a novel mechanism to activate vinculin. *J. Biol. Chem.* **287**, 7728–7737 (2012).
30. V. Bejar-Padilla, J. I. Cabe, S. Lopez, V. Narayanan, M. Mezher, V. Maruthamuthu, D. E. Conway, α-Catenin-dependent vinculin recruitment to adherens junctions is antagonistic to focal adhesions. *Mol. Biol. Cell* **33**, ar93 (2022).
31. A. E. Beedle, A. Williams, J. Relat-Goberna, S. Garcia-Manyes, Mechanobiology - chemical origin of membrane mechanical resistance and force-dependent signaling. *Curr. Opin. Chem. Biol.* **29**, 87–93 (2015).
32. P. Jin, L. Y. Jan, Y. N. Jan, Mechanosensitive ion channels: Structural features relevant to mechanotransduction mechanisms. *Annu. Rev. Neurosci.* **43**, 207–229 (2020).

33. R. Gnanasambandam, C. Ghatak, A. Yasmann, K. Nishizawa, F. Sachs, A. S. Ladokhin, S. I. Sukharev, T. M. Suchyna, GsMTx4: Mechanism of inhibiting mechanosensitive ion channels. *Biophys. J.* **112**, 31–45 (2017).
34. A. Faucherre, K. Kissa, J. Nargeot, M. E. Mangoni, C. Jopling, Piezo1 plays a role in erythrocyte volume homeostasis. *Haematologica* **99**, 70–75 (2014).
35. M. Oginuma, M. Nishida, T. Ohmura-Adachi, K. Abe, S. Ogamino, C. Mogi, H. Matsui, T. Ishitani, Rapid reverse genetics systems for *Nothobranchius furzeri*, a suitable model organism to study vertebrate aging. *Sci. Rep.* **12**, 11628 (2022).
36. L. H. K. Lim, S. Pervaiz, Annexin 1: The new face of an old molecule. *FASEB J.* **21**, 968–975 (2007).
37. M. de Graauw, M. H. van Miltenburg, M. K. Schmidt, C. Pont, R. Lalai, J. Kartopawiro, E. Pardali, S. E. Le Dévédec, V. T. Smit, A. van der Wal, L. J. Van't Veer, A. M. Cleton-Jansen, P. ten Dijke, B. van de Water, Annexin A1 regulates TGF-β signaling and promotes metastasis formation of basal-like breast cancer cells. *Proc. Natl. Acad. Sci. U.S.A.* **104**, 6340–6345 (2010).
38. H. L. Ashe, J. Briscoe, The interpretation of morphogen gradients. *Development* **133**, 385–394 (2006).
39. F. Huizar, D. Soundarrajan, R. Paravitorghabeh, J. Zartman, Interplay between morphogen-directed positional information systems and physiological signaling. *Dev. Dyn.* **249**, 328–341 (2020).
40. S. Hirano, Y. Mii, G. Charras, T. Michiue, Alignment of the cell long axis by unidirectional tension acts cooperatively with Wnt signalling to establish planar cell polarity. *Development* **149**, dev200515 (2022).
41. N. I. Petridou, S. Grigolon, G. Salbreux, E. Hannezo, C. P. Heisenberg, Fluidization-mediated tissue spreading by mitotic cell rounding and noncanonical Wnt signalling. *Nat. Cell Biol.* **21**, 169–178 (2019).
42. D. Pinheiro, R. Kardos, É. Hannezo, C. P. Heisenberg, Morphogen gradient orchestrates pattern-preserving tissue morphogenesis via motility-driven unjamming. *Nat. Phys.* **18**, 1482–1493 (2022).
43. A. Nagafuchi, M. Takeichi, Transmembrane control of cadherin-mediated cell adhesion: A 94 kDa protein functionally associated with a specific region of the cytoplasmic domain of E-cadherin. *Cell Regul.* **1**, 37–44 (1989).
44. T. Y. Tsai, M. Sikora, P. Xia, T. Colak-Champollion, H. Knaut, C. P. Heisenberg, S. G. Megason, An adhesion code ensures robust pattern formation during tissue morphogenesis. *Science* **370**, 113–116 (2020).
45. A. Matamoro-Vidal, R. Levayer, Multiple influences of mechanical forces on cell competition. *Curr. Biol.* **29**, R762–R774 (2019).
46. C. Brás-Pereira, E. Moreno, Mechanical cell competition. *Curr. Opin. Cell Biol.* **51**, 15–21 (2018).
47. C. J. Jou, K. W. Spitzer, M. Tristani-Firouzi, Blebbistatin effectively uncouples the excitation-contraction process in zebrafish embryonic heart. *Cell. Physiol. Biochem.* **25**, 419–424 (2010).
48. L. Marchant James, M. Smith Frank, P. F. Anthony, The effective use of blebbistatin to study the action potential of cardiac pacemaker cells of zebrafish (*Danio rerio*) during incremental warming. *Curr. Res Physiol.* **5**, 48–54 (2022).
49. A. E. E. Bruce, C. P. Heisenberg, Mechanisms of zebrafish epiboly: A current view. *Curr. Top. Dev. Biol.* **136**, 319–341 (2020).
50. P. Campinho, M. Behrndt, J. Ranft, T. Risler, N. Minc, C. P. Heisenberg, Tension-oriented cell divisions limit anisotropic tissue tension in epithelial spreading during zebrafish epiboly. *Nat. Cell Biol.* **15**, 1405–1414 (2013).
51. E. Perozo, A. Kloda, D. M. Cortes, B. Martinac, Physical principles underlying the transduction of bilayer deformation forces during mechanosensitive channel gating. *Nat. Struct. Biol.* **9**, 696–703 (2002).
52. S. E. Murthy, A. E. Dubin, A. Patapoutian, Piezos thrive under pressure: Mechanically activated ion channels in health and disease. *Nat. Rev. Mol. Cell Biol.* **18**, 771–783 (2017).
53. F. Antonicelli, C. De Coupade, F. Russo-Marie, Y. Le Garrec, CREB is involved in mouse annexin A1 regulation by cAMP and glucocorticoids. *Eur. J. Biochem.* **268**, 62–69 (2001).
54. K. W. Kinzler, M. C. Nilbert, L. K. Su, B. Vogelstein, T. M. Bryan, D. B. Levy, K. J. Smith, A. C. Preisinger, P. Hedge, D. McKechnie, R. Finniear, A. Markham, J. Groffen, M. S. Boguski, S. F. Altschul, A. Horii, H. Ando, Y. Miyoshi, Y. Miki, I. Nishisho, Y. Nakamura, Identification of FAP locus genes from chromosome 5q21. *Science* **253**, 661–665 (1991).
55. I. Nishisho, Y. Nakamura, Y. Miyoshi, Y. Miki, H. Ando, A. Horii, K. Koyama, J. Utsunomiya, S. Baba, P. Hedge, Mutations of chromosome 5q21 genes in FAP and colorectal cancer patients. *Science* **253**, 665–669 (1991).
56. M. H. Wong, B. Rubinfeld, J. I. Gordon, Effects of forced expression of an NH2-terminal truncated β-catenin on mouse intestinal epithelial homeostasis. *J. Cell Biol.* **141**, 765–777 (1998).
57. G. Christofori, H. Semb, The role of the cell-adhesion molecule E-cadherin as a tumour-suppressor gene. *Trends Biochem. Sci.* **24**, 73–76 (1999).
58. R. Derynck, R. J. Akhurst, A. Balmain, TGF-β signaling in tumor suppression and cancer progression. *Nat. Genet.* **29**, 117–129 (2001).
59. L. Parente, E. Solito, Annexin 1: More than an anti-phospholipase protein. *Inflam. Res.* **53**, 125–132 (2004).
60. A. Sabran, E. Kumolosasi, I. Jantan, Effects of annexin A1 on apoptosis and cell cycle arrest in human leukemic cell lines. *Acta Pharm.* **69**, 75–86 (2019).
61. N. Shimizu, K. Kawakami, T. Ishitani, Visualization and exploration of Tcf/Lef function using a highly responsive Wnt/β-catenin signaling-reporter transgenic zebrafish. *Dev. Biol.* **370**, 71–85 (2012).
62. C. L. Stoick-Cooper, G. Weidinger, K. J. Riehle, C. Hubbert, M. B. Major, N. Fausto, R. T. Moon, Distinct Wnt signaling pathways have opposing roles in appendage regeneration. *Development* **134**, 479–489 (2007).
63. H. Aberle, A. Bauer, J. Stappert, A. Kispert, R. Kemler, β-catenin isa target for the ubiquitin-proteasome pathway. *EMBO J.* **16**, 3797–3804 (1997).
64. U. Rescher, N. Zobiack, V. Gerke, Intact Ca^{2+}-binding sites are required for targeting of annexin 1 to endosomal membranes in living HeLa cells. *J. Cell Sci.* **113**, 3931–3938 (2000).
65. M. C. Subauste, M. Von Herrath, V. Benard, C. E. Chamberlain, T. H. Chuang, K. Chu, G. M. Bokoch, K. M. Hahn, Rho family proteins modulate rapid apoptosis induced by cytotoxic T lymphocytes and Fas. *J. Biol. Chem.* **275**, 9725–9733 (2000).
66. K. Yamamoto, H. Ichijo, S. J. Korsmeyer, BCL-2 is phosphorylated and inactivated by an ASK1/Jun N-terminal protein kinase pathway normally activated at G(2)/M. *Mol. Cell. Biol.* **19**, 8469–8478 (1999).
67. E. Kardash, M. Reichman-Fried, J. L. Maître, B. Boldajipour, E. Papusheva, E. M. Messerschmidt, C. P. Heisenberg, E. Raz, A role for Rho GTPases and cell-cell adhesion in single-cell motility in vivo. *Nat. Cell Biol.* **12**, 47–53 (2010).
68. H. Hashimoto, M. Itoh, Y. Yamanaka, S. Yamashita, T. Shimizu, L. Solnica-Krezel, M. Hibi, T. Hirano, Zebrafish Dkk1 functions in forebrain specification and axial mesendoderm formation. *Dev. Biol.* **217**, 138–152 (2000).
69. T. P. Stauffer, S. Ahn, T. Meyer, Receptor-induced transient reduction in plasma membrane PtdIns(4,5)P_2 concentration monitored in living cells. *Curr. Biol.* **8**, 343–346 (1998).
70. T. Shimizu, T. Yabe, O. Muraoka, S. Yonemura, S. Aramaki, K. Hatta, Y. K. Bae, H. Nojima, M. Hibi, E-cadherin is required for gastrulation cell movements in zebrafish. *Mech. Dev.* **122**, 747–763 (2005).
71. T. Hashimshony, N. Senderovich, G. Avital, A. Klochendler, Y. de Leeuw, L. Anavy, D. Gennert, S. Li, K. J. Livak, O. Rozenblatt-Rosen, Y. Dor, A. Regev, I. Yanai, CEL-Seq2: Sensitive highly-multiplexed single-cell RNA-Seq. *Genome Biol.* **17**, 77 (2016).
72. B. Langmead, S. L. Salzberg, Fast gapped-read alignment with Bowtie 2. *Nat. Methods* **9**, 357–359 (2012).
73. S. Anders, P. T. Pyl, W. Huber, HTSeq—A Python framework to work with high-throughput sequencing data. *Bioinformatics* **31**, 166–169 (2015).
74. S. X. Ge, E. W. Son, R. Yao, iDEP: An integrated web application for differential expression and pathway analysis of RNA-Seq data. *BMC Bioinform.* **19**, 534 (2018).
75. C. Thisse, B. Thisse, High-resolution in situ hybridization to whole-mount zebrafish embryos. *Nat. Protoc.* **3**, 59–69 (2008).
76. T. Brend, S. A. Holley, Zebrafish whole mount high-resolution double fluorescent in situ hybridization. *J. Vis. Exp.* **25**, 1229 (2009).

Acknowledgments: We thank K. Kawakami, A. Kikuchi, V. Gerke, U. Rescher, G. Bokoch, J. Ikenouchi, S. Korsmeyer, E. Raz, M. Hibi, J. Nakai, M. Glotzer, T. Meyer, and M. Tada for providing plasmids and Ishitani lab members for helpful discussions, technical support, and fish maintenance. **Funding:** This work was supported by Takeda Science Foundation (T.I.), SECOM Science and Technology Foundation (T.I.), KOSE Cosmetology Foundation (T.I.), The Nippon Foundation - Osaka University Project for Infectious Disease Prevention (T.I.), Grant-in-Aid for Transformative Research Areas (A) (21H05287, T.I.; and 23H04705, K.A.), Scientific Research (B) (22H02820) (T.I.), Challenging Exploratory Research (23K18242) (T.I.), Scientific Research on Innovative Areas (22H04845) (Y.A.), Early-Career Scientists (21K15085, Y.A.; and 22 K15104, K.A.), Grant-in-Aid for JSPS Fellows (21J01076) (K.A.), MEXT Promotion of Development of a Joint Usage/Research System Project: Coalition of Universities for Research Excellence (CURE) Program (JPMXP1323015484) (T.I.), and AMED-CREST (24gm2010001h0001) (T.I.). **Author contributions:** Conceptualization: K.A. and T.I. Methodology: K.A., T.H., Y.A., Y.O., and T.I. Investigation: K.A., T.H., Y.A., Y.O., and K.M. Visualization: K.A., T.H., and K.M. Funding acquisition: K.A., Y.A., and T.I. Project administration: K.A. and T.I. Supervision: T.I. Writing—original draft: K.A. and T.I. Writing—review and editing: K.A. and T.I. All authors have reviewed the manuscript. **Competing interests:** The authors declare that they have no competing interests. **Data and materials availability:** All data needed to evaluate the conclusions in the paper are present in the paper and/or the Supplementary Materials. The RNA-seq data are available from the National Center for Biotechnology Information GEO database under the accession code GSE254439.

Submitted 14 March 2024
Accepted 16 October 2024
Published 15 November 2024
10.1126/sciadv.adp2357